The thickness imaging of channels using multiple-frequency components analysis

Yan Ye[1], Bo Zhang[2], Cong Niu[3], Jie Qi[4], and Huailai Zhou[5]

Abstract

Blending of different frequency components of seismic traces is a common way to estimate the relative time thickness of the formation. Red, blue, and green (RGB) color blending is one of the most popular blending models in analyzing multiple seismic attributes. Geologists and geophysicist interpreters typically associate low-frequency components (formations with the largest thickness value) with a red color, medium-frequency components (formations with a medium thickness value) with a green color, and high-frequency components (formations with the smallest thickness value) with a blue color for the thickness estimation of thin beds using frequency components. However, we found that the same result of RGB blending may come from different sets of three frequency components. As a result, the same blended color may correspond to several different time thicknesses. It is also very difficult to interpret the corresponding thickness of the blended colors such as white and yellow. To avoid the ambiguity of time-thickness estimation using RGB blending, we have estimated the time thickness of the thin beds using all of the frequency components in a user-defined frequency band instead of only three frequency components. Our workflow begins with the normal seismic spectral decomposition. Considering that the different reflectivity pairs with a different time thickness have a different amplitude spectrum, we then use the self-organizing map to cluster the decomposed amplitude spectra of seismic traces. We finally assign each cluster with a relative thickness by comparing the clustered results with well logs.

Introduction

Quantitative thickness estimation of a thin-bed using seismic data is one of the most important tasks in reservoir characterization. The bandwidth of the seismic data is one of the key factors that determine the seismic resolution (Ricker, 1953a, 1953b). Widess (1973) concludes that the limit of detectable thickness for a single bed was $\lambda/8$ and obtains a linear relation between the reflection amplitude and the thickness of the thin bed. However, Kallweit and Wood (1982) point out that Widess's conclusion was based on visual inspection of the seismic amplitude and was not analytically correct. Kallweit and Wood (1982) show that the peak-to-trough time decreases with the decreasing thickness of the thin bed and develop a theoretical method to predict the thickness of the thin bed using frequency and time. Robertson and Nogami (1984) find that the instantaneous frequency was a sensitive analytical parameter in investigating the stratigraphic sequences composed of very thin layers. Chung and Lawton (1995) study four wedge models with different types of reflectivity and propose using the peak frequency to predict the thickness of thin beds.

Partyka et al. (1999) propose a turning point of thickness estimation methodology, which uses the features of the decomposed amplitude spectrum of seismic traces. Partyka et al. (1999) illustrate that the temporal thickness of thin beds equals the reciprocal of the period of the notches of the amplitude spectrum. Partyka (2001) illustrates that the amplitude of the seismic can be used to quantify thickness of the thin bed if the thickness of the thin bed is below the tuning thickness. Barnes et al. (2004) implement spectral decomposition using Gabor and Morlet wavelets and include that both decomposed spectrum results provide results for the qualitative interpretation and the thickness estimation. Zeng and Backus (2005a, 2005b) rotate the phase of the seismic volume by 90° and track the thin beds on the

[1]Chengdu University of Technology, College of Geophysics, Chengdu, China and The University of Alabama, Department of Geological Sciences, Tuscaloosa, Alabama 35401, USA. E-mail: yywsally@126.com.
[2]The University of Alabama, Department of Geological Sciences, 2003 Bevill Building, Tuscaloosa, Alabama 35401, USA. E-mail: bzhang33@ua.edu (corresponding author).
[3]CNOOC Research Institute, Beijing, China. E-mail: niucong@cnooc.com.cn.
[4]The University of Oklahoma, ConocoPhillips School of Geology and Geophysics, Norman, Oklahoma, USA. E-mail: jie.qi@ou.edu.
[5]Chengdu University of Technology, College of Geophysics, Chengdu, China. E-mail: zhouhuailai06@cdut.cn.

Manuscript received by the Editor 8 March 2018; revised manuscript received 8 August 2018; published ahead of production 13 October 2018; published online 8 January 2019. This paper appears in *Interpretation*, Vol. 7, No. 1 (February 2019); p. B1–B8, 14 FIGS.
http://dx.doi.org/10.1190/INT-2018-0064.1.

phase-rotated seismic volume. Zeng and Backus (2005a, 2005b) conclude that it is much simpler to characterize the thin beds on the phase-rotated seismic volumes. Hall (2006) proposes an approach called cepstral decomposition to measure the bed thickness. Liu and Marfurt (2006) show that the peak frequency can give a reasonably good estimate of thickness if the bed thickness is less than the tuning thickness when given adequate well control. Khare and Martinez (2008) demonstrate that amplitude ratios of frequencies can be used as an indicator of thickness variations. Oyem and Castagna (2013) test the accuracy of short time window Fourier transform and constrain least-squares spectral analysis (CLSSA) spectra in determining the time thicknesses of thin beds. Oyem and Castagna (2013) show that CLSSA yields more accurate layer thickness estimation. Wallet (2016) illustrates that the peak-to-trough (or trough-to-trough) time corresponds to the approximate frequency. Wallet (2016) states that it is feasible to use the spectral decomposition attributes to generate 3D geologic modeling of channels. Zhou and Castagna (2017) use the principal component of the amplitude spectrum of seismic to map the thickness of the channels. Yuan et al. (2017) propose a sparse Bayesian learning-based time-variant deconvolution method to avoid the thin-layer artifacts associated with stationary deconvolution.

Red-green-blue (RGB) blending is one of the most popular multiple seismic attribute analysis methods. Balch (1971) proposes to characterize the reservoir properties by RGB blending the low-, medium-, and high-frequency components of the amplitude spectrum of seismic data. Liu (2006) blends peak frequency, peak amplitude, and coherence attributes using RGB strategy to highlight the discontinuities and thickness variation of the reservoir. Guo et al. (2008) propose a multiple attribute mapping strategy by using 3C and 4C models. Laake (2015) proposes an RGB processing method called structure-sharpened continuous RGB (SRGB). The SRGB method used continuous RGB color to render multiple data layers at the same time and to provide a visual environment of geologic features for the interpreters. Zeng (2017) estimates the thickness and shale contents of thin beds by using the results of color-blended multiple frequencies. Selecting the proper low-, medium-, and high-frequency components is the most challenging task in thin-bed characterization using the RGB blending technologies. Researchers usually define the "low-", "medium-," and "high-"frequency components according to their intuitive experience.

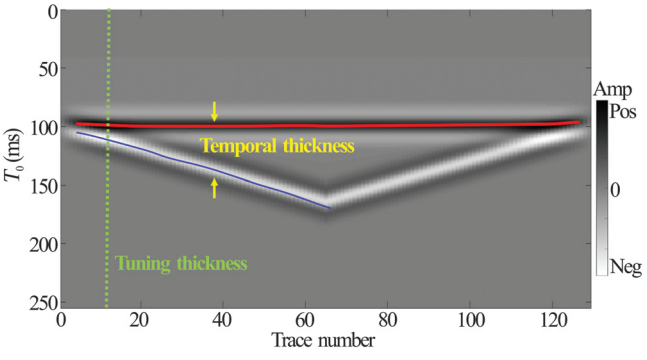

Figure 1. Channel model. The top of the channel is at time 100 ms. The channel thickness from 1 ms on the left and reaches the thickest at 65 ms.

To improve the accuracy and stability of the thickness estimation of thin beds, we propose to estimate the time thickness of the thin beds using all of the frequency components within a user-defined frequency band. Our paper begins with reviewing the thickness estimation approaches. We then use a simple wedge model to illustrate the process of thickness estimation of a thin bed using the peak frequency. We next examine the accuracy of RGB blending of three frequency components in mapping the thickness of thin beds. We finally propose our workflow to mapping the time thickness of a thin bed by using all of the frequency components within a user-defined bandwidth. Our workflow uses the self-organizing map (SOM) to build the relationship between the multiple-frequency components and the time thickness of thin beds. To illustrate the effectiveness of our method, we first apply our method to a wedged synthetic model and then to a seismic survey acquired over the eastern part of the Anadarko Basin, Oklahoma.

Thickness estimation of a thin bed

The methods used to characterize the thickness of a thin bed can be categorized in the following four categories: (1) the two-way time difference between the interpreter tracked horizons, (2) methods based on the tuning features of seismic amplitude, (3) methods using a single frequency component of seismic data, and (4) methods blending the multiple frequency components of seismic data. In this paper, we generated a synthetic channel model to demonstrate the effectiveness of the thickness estimation methods. Each trace of our model consists of two opposite but equal reflectivity spikes. The maximum and minimum two-way time thickness of our channel is 65 and 0 ms. Figure 1 shows the seismogram of the synthetic channel model by convolving the reflectivity model with a 35 Hz Ricker wavelet. There are 129 seismic traces in our synthetic model, and the time-sampling rate is 1 ms.

Thickness estimation using the seismic amplitude

The red and blue curves in Figure 1 show the peak and trough of the seismic events, respectively. The green curve indicates the seismic trace with the tuning thickness. The black curve in Figure 2 is the time thickness between the peak (red curve in Figure 1) and trough (blue curve in Figure 1) of the seismic events. Note that the time thickness between the peak and trough perturbs at approximately 10 ms if the time thickness of the channel is smaller than the tuning thickness. This phenomenon indicates that the peak-to-trough time thickness is incapable of resolving the thickness of a thin bed if the thickness is smaller than the tuning thickness.

Assume that the source wavelet is a Ricker wavelet (Ricker, 1953a), which can be expressed as

$$A(t) = [1 - 2(\pi f_p t)^2] \exp[-(\pi f_p t)^2], \quad (1)$$

where t is the time and f_p is the peak frequency, which is defined as the frequency with the largest amplitude. We can set the derivative of the amplitude to zero to get the tuning thickness (Kallweit and Wood, 1982):

$$\frac{dA(t)}{dt} = 2(\pi f_p)^2 t[2(\pi f_p t)^2 - 3] \exp[-(\pi f_p t)^2] = 0. \quad (2)$$

Then, the tuning thickness h_t for a Ricker wavelet is given by

$$h_t = \frac{1}{2.6 * f_p}. \quad (3)$$

The peak frequency of our wavelet is 35 Hz. Then, the tuning thickness is 11 ms according to equation 3 in our model. The red curve in Figure 2 is the amplitude of the peaks of the seismic reflection. The amplitude reaches a maximum value if the time thickness of the channel equals tuning thickness. However, we usually do not use the amplitude to characterize the time thickness of the thin bed due to its sensitivity to noise.

Thickness estimation using single-frequency component of seismic data

Researchers have used the first dominant frequency of the decomposed amplitude spectrum of seismic data in mapping the time thickness of the thin bed. In this paper, we use the S-transform to decompose the seismic traces. The black and red curves in Figure 3 are the first dominant frequency and corresponding amplitude of the first dominant frequency, respectively. Figure 3 shows that the tuning thickness is related to the dominant amplitude and dominant frequency. We can use the amplitude of the first dominant frequency to estimate the time thickness if the time thickness of the bed is less than the tuning thickness. We can use the dominant frequency to estimate the time thickness if the time thickness of the bed is greater than the tuning thickness. We also notice that there is a significant "staircase" phenomenon for the first dominant frequency. The staircase phenomenon would lower the accuracy of the time-thickness estimation. Stability is another factor that hinders the wide application of using a single-frequency component in mapping the time thickness of the thin bed. The noise contained in the seismic data also affects the amplitude spectrum of seismic data, which further affect the distribution of the first dominant frequency. The artifacts introduced by processing, such as stretching, may also affect the distribution of the first dominant frequency.

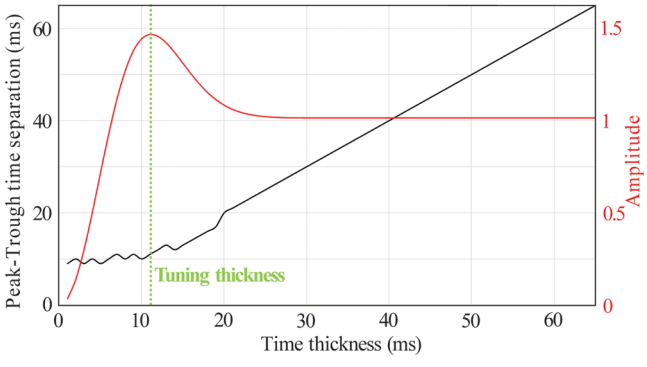

Figure 2. Tuning analysis. The peak-to-trough time is the apparent channel thickness between the peak and trough, and the amplitude is the amplitude difference between the maximum (peak) and minimum (trough) value.

Thickness estimation using RGB blending of multiple-frequency components of seismic data

To compensate the disadvantages of mapping the time thickness of thin bed, researchers combine several frequency components to characterize the thin bed. RGB blending is one of the most used strategies used for displaying multiple-frequency components. RGB blending is an additive color model using the primary colors of red, green, and blue to reproduce a broad array of colors tuning with human vision perceptions.

The RGB blending basic functions can be written as (Liu, 2006)

$$b_R(f) = 0.5 \cdot \left(1.0 + \cos\left(\pi \frac{f - f_R}{k \cdot f_{\text{Bandwidth}}}\right)\right), \quad (4a)$$

$$b_G(f) = 0.5 \cdot \left(1.0 + \cos\left(\pi \frac{f - f_G}{k \cdot f_{\text{Bandwidth}}}\right)\right), \quad (4b)$$

$$b_B(f) = 0.5 \cdot \left(1.0 + \cos\left(\pi \frac{f - f_B}{k \cdot f_{\text{Bandwidth}}}\right)\right), \quad (4c)$$

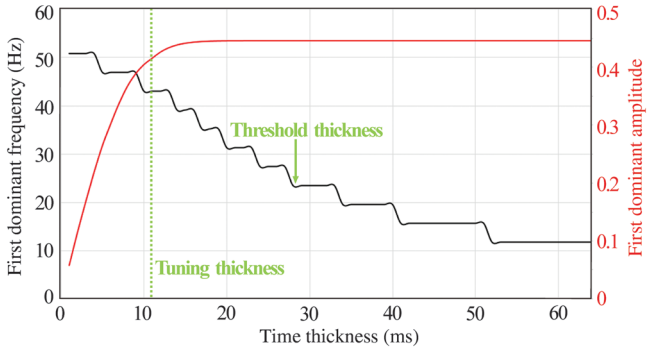

Figure 3. The first dominant amplitude versus first dominant frequency. The dominant amplitude can be used to estimate the thickness when the bed is below the tuning thickness. The dominant frequency can be used to estimate the thickness that is greater than the tuning thickness.

where $b_R(f)$, $b_G(f)$, and $b_B(f)$ are the basic functions of the red, green, and blue colors in RGB blending and f_R, f_G, and f_B are the center frequencies for the red, green, and blue colors basic functions, respectively. Here, $f_{\text{Bandwidth}}$ is the frequency bandwidth of the seismic data and k is a constant that controls the bandwidth of the cosine function.

We can write these basic functions as a matrix $\mathbf{B}$:

$$\mathbf{B} = \begin{bmatrix} b_R(f_1) & b_G(f_1) & b_B(f_1) \\ b_R(f_2) & b_G(f_2) & b_B(f_2) \\ \vdots & \vdots & \vdots \\ b_R(f_m) & b_G(f_m) & b_B(f_m) \end{bmatrix}. \quad (5)$$

We use least-squares to match the RGB's three basic functions to the decomposed amplitude spectrum of the seismic data:

$$\mathbf{C} = [\mathbf{B^T B} + \varepsilon \mathbf{I}]^{-1} \mathbf{B^T} \cdot \mathbf{U}, \quad (6)$$

where vectors $\mathbf{C} = \begin{pmatrix} c_R \\ c_G \\ c_B \end{pmatrix}$ is the RGB coefficients vector, $\mathbf{U} = \begin{pmatrix} u(f_1) \\ u(f_2) \\ \vdots \\ u(f_m) \end{pmatrix}$ is the spectral components vector, $\mathbf{I}$ is an 3 x 3 identity matrix, and ε is a small number that stabilizes the solution.

We first extract the amplitude spectrum of the seismic data along the red horizon shown in Figure 1. We then RGB blend three frequency components (20, 40, and 60 Hz) to characterize the thickness of the channel. Figure 4 shows the RGB blending result. The RGB blending in assisting the thin-bed characterization has the following three assumptions. The red color is associated with low frequency, which stands for a larger time thickness. The green color is associated with medium frequency, which stands for a medium time thickness. The blue color is associated with high frequency, which stands for a small time thickness. Note that the RGB blending result has very good correlation with our time thickness of the synthetic model. But we do have several disagreements indicated by the arrows in Figure 4. There is no definition about the time thickness for the zone represented by yellow (indicated by the yellow arrow in Figure 4) and purple colors (indicated by the purple arrow in Figure 4). The time thickness of the channel indicated by the green arrow is larger than the time thickness of the channel indicated by the red arrow. Unfortunately, this fact conflicts with our assumption of RGB blending strategy.

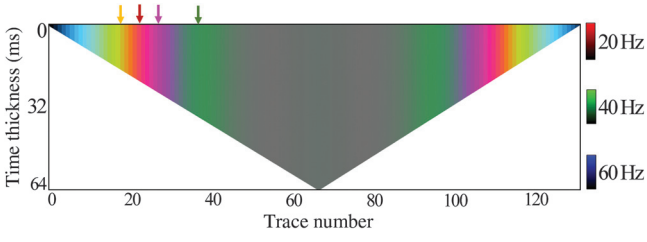

Figure 4. The RGB blending result. The 20 Hz component is plotted against red, 40 Hz component is plotted against green, and the 60 Hz component is plotted against blue. There are some zones indicated by arrows that conflict with our assumption of the RGB blending strategy.

Figure 5 illustrates the amplitude variation of certain frequency component with the time thickness of the channel. The red, green, and blue curves are the amplitude of 10, 20, and 30 Hz, respectively. Figure 5 indicates the "confused" phenomenon shown in Figure 4. The amplitude value of 0.4 has a unique corresponding time thickness (10 ms) for the 10 Hz component. However, the amplitude value of 0.4 has three corresponding time thicknesses for the 20 and 30 Hz components. The nonunique relationship between amplitude value and time thickness would introduce ambiguity in the following RGB blending. As a result, channels with different time thicknesses may have the same RGB blending color scheme.

Thickness estimation by clustering the multiple-frequency components of seismic data

Figure 6 shows the decomposed amplitude spectrum of several representative seismic traces. Note that the amplitude of different seismic traces (different time thickness) have different features. The difference between the curve shapes of the spectrum is obvious enough to differentiate with each other. Based on this observation, we propose mapping the time thickness of a thin bed by clustering the decomposed amplitude spectrum of the seismic traces.

In this paper, we choose the SOM (Kohonen, 1982) as the clustering method. SOM becomes a widely used unsupervised network, and researchers have successfully applied SOM to multiple attribute analysis. Poupon et al. (1999) perform one of the earliest SOM-based seismic facies analyses, and they find that the shape variation of seismic traces is a good indicator of the sand thick-

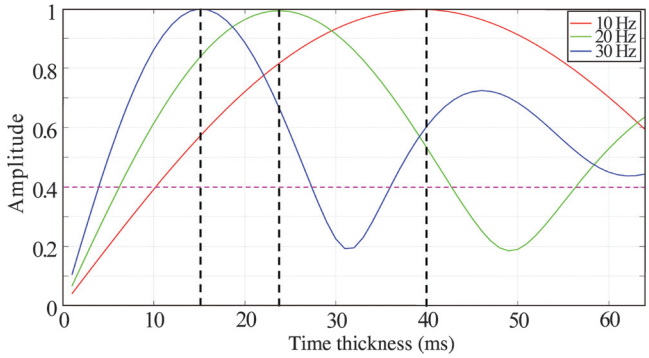

Figure 5. Spectral amplitude concerning the time thickness. The amplitude variation of certain frequency component with the time thickness of the channel. It indicates the confused phenomenon shown in Figure 4.

ness as well as the gas saturation. Strecker and Uden (2002) cluster poststack seismic attributes into four different Kohonen SOM runs. Strecker and Uden (2002) find that the clustered result helps the geologic interpreters to extract more stratigraphic details. Zhao et al. (2016) characterize a Miocene deepwater turbidite system by applying the SOM to multiple seismic attributes. Hardisty and Wallet (2017) improve the SOM perform on multiple seismic attributes analysis by modifying the input of the Gaussian mixture models. Ha et al. (2017) apply a SOM classification to multiple seismic attributes to highlight hydrocarbon-related facies.

The Kohonen SOM network has an input layer and a competitive layer. The weight vector for each SOM neuron is $\mathbf{w}_{ji} = [\mathbf{w}_{j1} \quad \mathbf{w}_{j2} \quad \mathbf{w}_{j3} \quad \ldots \quad \mathbf{w}_{jn-1} \quad \mathbf{w}_{jn}]$, where i is an SOM neuron in the input layer and j is an SOM neuron in the competitive layer. These neurons or prototype vectors (PVs) are arranged in a regular low-dimensional grid or map (1D, 2D, or 3D). The input for SOM is a set of attribute vectors $\mathbf{X} = [\mathbf{x}_1 \quad \mathbf{x}_2 \quad \mathbf{x}_3 \quad \ldots \quad \mathbf{x}_{n-1} \quad \mathbf{x}_n]$, and each attribute vector $\mathbf{x}_i$ contains m attributes. The purpose of SOM analysis is to classify the attribute vector set into different groups. During the process of SOM, the distance between input vectors and the weight vector will be calculated, usually using the Euclidean metric: $d_j = \sqrt{\sum_{i=1}^{n}(\mathrm{X}_i - \mathrm{W}_{ji})^2}$. The "winner" PV is defined as the best-matching vector that has the minimum distance to the input (most similar to the input). After the winner PV and the neighborhood around the winner are updated, the weights for all of the PVs in the neighborhood will be updated. The winner PV and its neighborhood have their weights modified to become more likely to win the competition and become the new cluster center. The next step is to change the best matching vector and the neighborhood's weight vector by taking the winner as the new center and iteratively updating the winner PVs to be closer to the input. The iteration will stop until the neighborhood radius decreases to the minimum distance between the PVs in the SOM grid space. Finally, we will assign the SOM result with the gradient color display. To facility the display (a colorbar that varies monotonically in a certain direction), we use a one-dimension topology instead of two dimensions for SOM. Figure 7 illustrates a typical decomposed amplitude spectrum. We arrange the value of the amplitude spectrum into a vector $\mathbf{a} = (a_1 \quad a_2 \quad a_3 \quad \ldots \quad a_{n-1} \quad a_n)$, and the vector $\mathbf{a}$ is the input for the SOM classification.

Figure 8 shows the clustered results by applying SOM to the amplitude spectrum of seismic data. The bandwidth used for the clustering is 10–70 Hz, and there are 64 clusters in our model. The red color indicates that the channels have a thick time thickness, and the blue color indicates that the channels have a thin time thickness. Note that we do not have ambiguity about the time thickness indicated by the color.

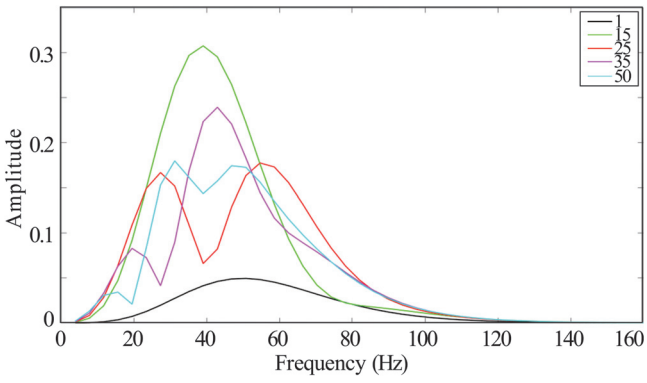

Figure 6. The decomposed amplitude spectrum of the representative seismic traces. The legend represents different seismic trace numbers. The amplitude of different seismic traces (different time thickness represented by different colors) have different features.

Field application

The study survey is located in the eastern part of the Anadarko Basin, Oklahoma (Figure 9). The depth of the target zone is at an approximate depth of 2680 m (approximately 8800 ft). The target zone is the Red Fork Sand of the middle Pennsylvanian and is composed of clastic facies deposited in a deep-marine (shale/silt) to shallow-water fluvial-dominated environment. The Red Fork Sandstone is sandwiched between limestone layers, with the Pink Limestone on top and the Inola Limestone on the bottom.

We first apply the S-transform to obtain the time-frequency spectrum of the seismic data. Figure 10 shows

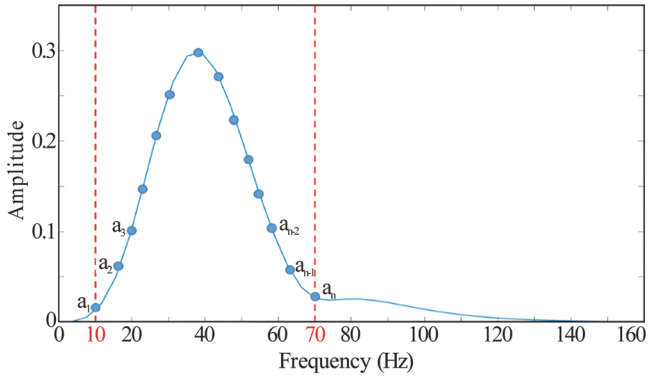

Figure 7. The input for the SOM classification.

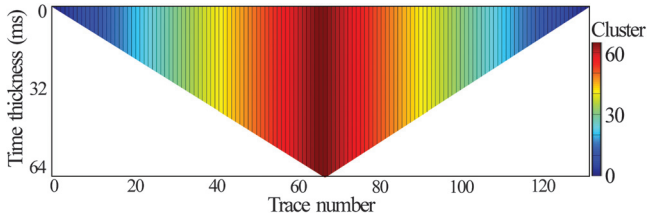

Figure 8. The clustered results by applying SOM to the amplitude spectrum of seismic data. The red and blue colors indicate that the channels have a thick time thickness and a thin time thickness, respectively.

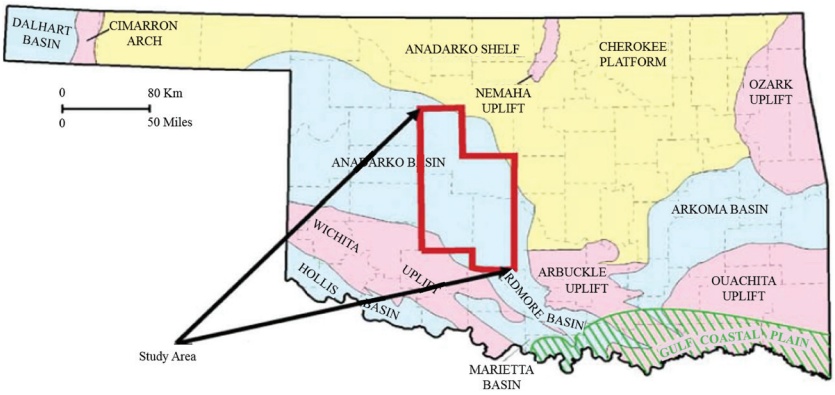

Figure 9. The location map of the Anadarko Basin area on a map of Oklahoma. The study survey is inside the area marked by the red boundary.

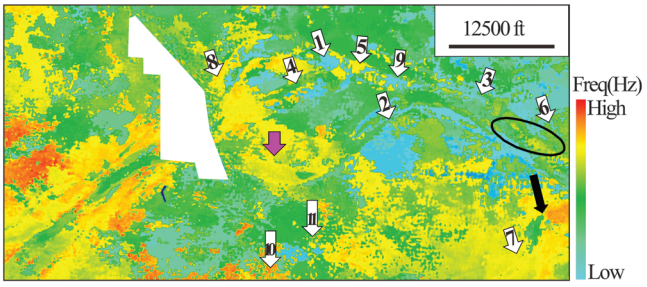

Figure 10. The peak frequency of the amplitude spectrum along the top of the Red Fork Formation.

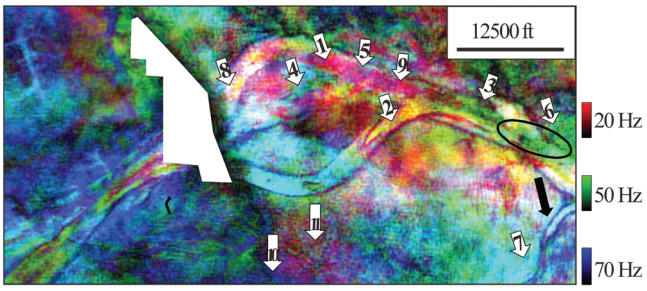

Figure 11. The RGB blending result of three selected frequency components. The 20 Hz in red, 50 Hz in green, and 70 Hz in blue.

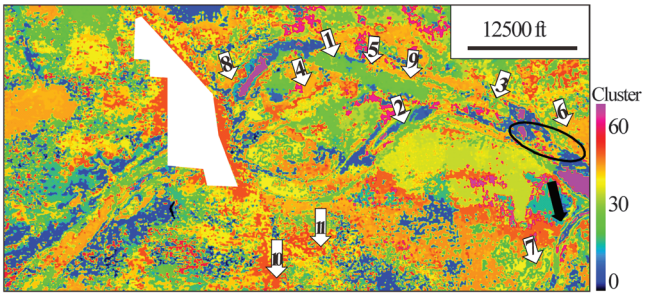

Figure 12. The clustered results of multiple-frequency components using SOM.

the peak frequency of the amplitude spectrum along the top of the Red Fork Formation. Note that the peak frequency successfully highlights the channel at most of the locations, but it fails to outline the channel indicated by the purple arrow. Figure 11 is the RGB-blending image of three frequency components. The selected three frequency components are 20 (red), 50 (green), and 70 Hz (blue), respectively. Note that the RGB blending result successfully highlights channels and channel edges. Figure 12 is the clustered results of multiple frequency components using SOM. The minimum and maximum frequency component are 10 and 70 Hz, respectively. The frequency sampling rate is approximately 2 Hz, and there are 32 frequency components used for clustering. There are 64 clusters in our clustering mode. Note that the clustered results illustrate the channel system.

We have 135 wells in our study area (Figure 13). Figure 14 shows the interpolated thickness of the Red Fork Formation using the well tops of Red Ford and Pink Lime. We observed a very good match between the patterns shown in Figures 12 and 14. For example, the locations pointed out by arrows 1–3 in Figure 14 belong to the same thickness (a small time thickness), and these locations are the same clustered results in Figure 12.

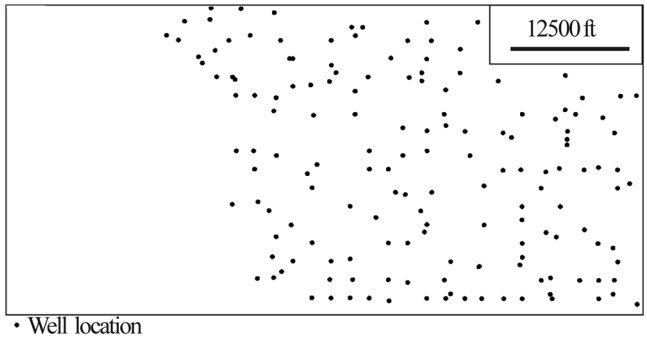

Figure 13. Well locations in our study area.

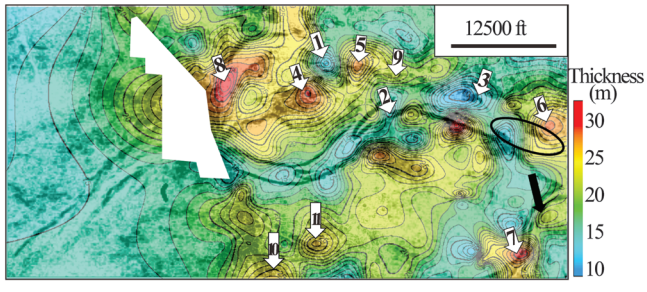

Figure 14. The multiattribute display of thickness contour map and coherence. The contour map is the interpolated thickness of the Red Fork Formation using two well tops (Red Fork and Pink Lime).

The locations pointed out by arrows 4–7 in Figure 12 are clustered to the same stage, meanwhile they are the same thickness in Figure 14. Note that the narrow branch channel indicated by the black arrow at the lower right in Figure 12 reveals the change of thickness. However, we find an ambiguity about the time thickness indicated by Figures 10 and 11. Arrow 1 indicates a small time thickness in Figure 14, whereas the location pointed out by arrow 1 denotes low frequency, which stands for a larger time thickness in Figure 10. The locations pointed out by arrows 7 and 8 in Figure 10 indicate a smaller time thickness with a higher frequency, but these two locations indicate a larger time thickness in Figure 14. There are also several disagreements indicated in Figure 11. Arrows 1, 5, and 9 in Figure 11 are all indicated by the red color standing for the same larger time thickness, whereas the channels pointed out by these three arrows are not supposed to have the same time thickness in Figure 14.

Arrows 1 and 3 denote the same time thickness in Figure 14, but Figure 11 shows different colors responding to different time thicknesses. The location pointed out by arrows 3 and 6 in Figure 11 are both indicating a medium time thickness with the green color, whereas there are smaller time thicknesses and larger time thicknesses in Figure 14, respectively. Moreover, the locations pointed out by arrows 5–7 are larger time thicknesses in Figure 14, but these locations in Figure 11 are denoted by different frequencies standing for different time thickness. The locations pointed out by arrows 5, 6, 10, and 11 are the same thickness in Figure 14, and these locations are also clustered to the same stage in Figure 12. But in Figure 11, these locations are displayed by different frequency components standing for different time thicknesses. In addition, the area in the black circle on the right is shown in the same color standing for the similar time thicknesses in Figure 11, whereas the thickness of this area is diverse in Figure 14.

Conclusion

Quantitative thickness estimation of thin bed is important in reservoir characterization. We can use the amplitude and frequency features of seismic data to estimate the time thickness of the thin bed. In this paper, we have discussed four methods used to estimate the time thickness of a thin bed with the goal of improving the accuracy and stability of the thickness estimation. However, the amplitude-based and single frequency feature-based methods are sensitive to noise. The RGB blending can only combine three frequency components, and it is very hard to choose the proper frequency components. We also have ambiguity in the interpretation of some of the blended colors, such as white and yellow. To use information contained by all the frequency components, we cluster the multiple-frequency components of seismic data by using SOMs. The clustered results are much closer to the interpolated thickness of the target formation using the well tops.

Acknowledgments

The first author appreciates the financial support from the National Science and Technology major project topic (2016ZX05026-001-005).

Data and materials availability

Data associated with this research are available and can be obtained by contacting the corresponding author.

References

Balch, A. H., 1971, Color sonograms: A new dimension in seismic data interpretation: Geophysics, **36**, 1074–1098, doi: 10.1190/1.1440233.

Barnes, A. E., L. Fink, and K. Laughlin, 2004, Improving frequency domain thin bed analysis: 74th Annual International Meeting, SEG, Expanded Abstracts, 1929–1932.

Chung, H. M., and D. C. Lawton, 1995, Frequency characteristics of seismic reflections from thin bed: Canadian Journal of Exploration Geophysics, **31**, 32–37.

Guo, H., S. Lewis, and K. J. Marfurt, 2008, Mapping multiple attributes to three- and four-component color models — A tutorial: Geophysics, **73**, no. 3, W7–W19, doi: 10.1190/1.2903819.

Ha, T., B. C. Wallet, and K. J. Marfurt, 2017, Seismic interpretation of the Exmouth Plateau, North Carnarvon Basin, Australia: An application of data conditioning, seismic attributes, and self-organizing map on 2D data: 87th Annual International Meeting, SEG, Expanded Abstracts, 2117–2121.

Hall, M., 2006, Predicting bed thickness with cepstral decomposition: The Leading Edge, **25**, 199–204, doi: 10.1190/1.2172313.

Hardisty, R., and B. C. Wallet, 2017, Unsupervised seismic facies from mixture models to highlight channel feature: 87th Annual International Meeting, SEG, Expanded Abstracts, 2289–2293.

Kallweit, R. S., and L. C. Wood, 1982, The limits of resolution of zero-phase wavelets: Geophysics, **47**, 1035–1046, doi: 10.1190/1.1441367.

Khare, V., and A. Martinez, 2008, Estimation of sub-tuned reservoir thickness from amplitudes at different seismic bandwidths: A time-domain approach: 78th Annual International Meeting, SEG, Expanded Abstracts, 2968–2972.

Kohonen, T., 1982, Self-organized formation of topologically correct feature maps: Biological Cybernetics, **43**, 59–69, doi: 10.1007/BF00337288.

Laake, A., 2015, Structural interpretation in color — A new RGB processing application for seismic data: Interpretation, **3**, no. 1, SC1–SC8, doi: 10.1190/INT-2014-0041.1.

Liu, J., 2006, Spectral decomposition and its application in mapping stratigraphy and hydrocarbons: Ph.D. thesis, University of Houston.

Liu, J., and K. J. Marfurt, 2006, Thin bed thickness prediction using peak instantaneous frequency: 76th Annual International Meeting, SEG, Expanded Abstracts, 968–972.

Oyem, A., and J. P. Castagna, 2013, Layer thickness estimation from the frequency spectrum of seismic reflection data: 83rd Annual International Meeting, SEG, Expanded Abstracts, 1451–1455.
Partyka, G. A., 2001, Seismic thickness estimation: Three approaches, pros and cons: 71st Annual International Meeting, SEG, Expanded Abstracts, 503–506.
Partyka, G. A., J. M. Gridley, and J. Lopez, 1999, Interpretational applications of spectral decomposition in reservoir characterization: The Leading Edge, **18**, 353–360, doi: 10.1190/1.1438295.
Poupon, M., K. Azbel, and G. Palmer, 1999, A new methodology based on seismic facies analysis and litho-seismic modeling: The Elkhorn Slough field pilot project, Solano County, California: 69th Annual International Meeting, SEG, Expanded Abstracts, 927–930.
Ricker, N., 1953a, The form and laws of propagation of seismic wavelets: Geophysics, **18**, 10–40, doi: 10.1190/1.1437843.
Ricker, N., 1953b, Wavelet contraction, wavelet expansion, and the control of seismic resolution: Geophysics, **18**, 769–792, doi: 10.1190/1.1437927.
Robertson, J. D., and H. H. Nogami, 1984, Complex seismic trace analysis of thin beds: Geophysics, **49**, 344–352, doi: 10.1190/1.1441670.
Strecker, U., and R. Uden, 2002, Data mining of 3D post-stack attribute volumes using Kohonen self-organizing maps: The Leading Edge, **21**, 1032–1037, doi: 10.1190/1.1518442.
Wallet, B. C., 2016, Is spectral decomposition suitable for 3D modeling of channels?: 86th Annual International Meeting, SEG, Expanded Abstracts, 2007–2011.
Widess, M. B., 1973, How thin is a thin bed?: Geophysics, **38**, 1176–1180, doi: 10.1190/1.1440403.
Yuan, S. Y., S. X. Wang, M. Ma, Y. Z. Ji, and L. Deng, 2017, Sparse Bayesian learning-based time-variant deconvolution: IEEE Transactions on Geoscience and Remote Sensing, **55**, 6182–6194, doi: 10.1109/TGRS.2017.2722223.
Zeng, H., 2017, Thickness imaging for high-resolution stratigraphic interpretation by linear combination and color blending of multiple-frequency panels: Interpretation, **5**, no. 3, T411–T422, doi: 10.1190/INT-2017-0034.1.
Zeng, H., and M. M. Backus, 2005a, Interpretive advantages of 90°-phase wavelets. Part 1: Modeling: Geophysics, **70**, no. 3, C7–C15, doi: 10.1190/1.1925740.
Zeng, H., and M. M. Backus, 2005b, Interpretive advantages of 90°-phase wavelets. Part 2: Seismic application: Geophysics, **70**, no. 3, C17–C24, doi: 10.1190/1.1925741.
Zhao, T., J. Zhang, F. Li, and K. J. Marfurt, 2016, Characterizing a turbidite system in Canterbury Basin, New Zealand, using seismic attributes and distance-preserving self-organizing maps: Interpretation, **4**, no. 1, SB79–SB89, doi: 10.1190/INT-2015-0094.1.
Zhou, J., and J. P. Castagna, 2017, Seismic thickness delineation using spectral principal component analysis theory and a synthetic turbidite example: 87th Annual International Meeting, SEG, Expanded Abstracts, 3158–3162.

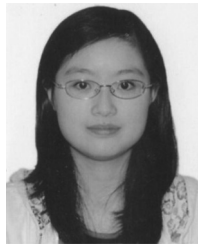

Yan Ye received a B.S. (2012) in exploration technology and engineering and an M.S. (2015) in geodetection and information technology from the Chengdu University of Technology, where she is pursuing a Ph.D. in geodetection and information technology. Her current research interests include seismic inversion and seismic attribute analysis.

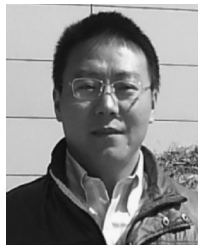

Huailai Zhou received a Ph.D. (2009) in earth exploration and information techniques from the Chengdu University of Technology. He completed his postdoctoral research within the Institute of Sedimentary Geology at the Chengdu University of Technology from 2010 to 2012. He was sponsored by the China Scholarship Council to work as postdoctoral research faculty in AASPI at the University of Oklahoma, USA, from October 2013 to October 2014. He currently works at the Chengdu University of Technology as a professor, and his research work is mainly focused on seismic data processing methods, seismic modeling and imaging, techniques of improving seismic resolution, and seismic attribute analysis and inversion methods.

Biographies and photographs of the other authors are not available.